ORIGINAL ARTICLES

Blind Median Filtering Detection Using Auto-Regressive Model and Markov Chain

Anjie Peng, Gao Yu, Hui Zeng*

School of Computer Science and Technology, Southwest University of Science and Technology, Mianyang, China

Received: July 11, 2018 **Accepted:** July 25, 2018 **Online Published:** August 10, 2018
DOI: 10.5430/ijrc.v1n1p32 **URL:** https://doi.org/10.5430/ijrc.v1n1p32

ABSTRACT

Establishing the processing history of an image is important for robot vision. In this paper, an improved method for median filtering detection is proposed. That is, detect whether an image has been processed by median filtering. First, we analyze the statistical properties of median filtering residual and find that it is suitable for exposing fingerprints of median filtering. Then, the new feature set on median filtering residual is constructed by incorporating transition probability matrices of Markov chain with coefficients of auto-regressive model. A dimensionality reduction method is developed to lower the feature dimensionality. The final feature set is fed into support vector machines to construct a detector. Due to the distinction property of median filtering residual as well as compensated effect between transition probability and auto-regressive model, experimental results on large image database demonstrate that the proposed method is effectively in median filtering detection, even for images with heavy JPEG compression or at a low resolution. The performance of proposed detector outperforms prior arts. Additionally, the proposed method demonstrates good generalization ability.

Key Words: Digital image forensics, Median filtering, Auto-regressive model, Transition probability

1. INTRODUCTION

Digital image processing is an important part of robot vision. When a low-quality image input into a robot, it need to be operated by image processing algorithm (such as image enhancement, image restoration etc.) to improve image quality. The processing history of an image may affect the effect of subsequent processing operation. Therefore, an automatically blind tool for detecting processing history of an image is necessary for robot vision. A great deal of attention has been paid on exposing history of digital image, such as the detection of median filtering,[1–5] re-sampling,[6] compression.[7] Revealing the processing history is also helpful for verifying the authenticity of an image.

Median filtering is a popular noise removal tool, which can effectively remove salt & pepper noise while reserving image details. A number of works have been proposed for median filtering detection. Kirchner and Fredrich utilized first-order difference to analyze streaking artifacts discovered by Bovik.[8] They proposed a robust detector using subtractive pixel adjacency matrix (SPAM) feature set and obtained reliable results for un-compressed images or moderate JPEG compressed images.[2] Cao et al. found that the probability of zero bins in textured region at the first-order was statistical different between original image and median filtering image.[3] They detected median filtering with high accuracy in the case of a median filtering image versus an original image. As median values originating from over-

*Correspondence: Hui Zeng; Email: zengh5@mail2.sysu.edu.cn; Address: School of Computer Science and Technology, Southwest University of Science and Technology, Mianyang, China.

lapping filtering windows are dependent upon each other, Yuan[4] proposed a blind forensic method based on above local dependence and constructed a feature set MFF with 44 dimensions, which achieved reliable results even for a low-resolution image or moderate JPEG compressed images. Chen et al. concatenated global probability feature set and local correlation feature set (GLF) on difference domain and obtained an excellent detector.[5]

The challenging problem for median filtering detection is dealing with image undergone heavy JPEG compression. The mentioned above prior works[2–5] capture fingerprints directly from pixels or difference domains and are easily disturbed by image content, therefore their detection performances decrease sharply for heavy JPEG compression. To eliminate interference from image compression, our previous work constructed the feature set on median filtering residual by auto-regressive (AR) model.[1] With only 10-D feature set, AR method achieves more robust performance to JPEG compression than GLF and MFF. However, the AR model describes dependence between adjacent residuals in a global way, thus loses some detailed information at small value elements, such as 0, -1, 1. We find that it is hard to improve detection accuracy further by only using AR model. Yang et al. employed two-dimensional autoregressive (2D-AR) model to extract a composite feature set from median filtered residual, average filtered residua and Gaussian filtered residual.[9] Their method outperforms 1-D AR model a lot for JPEG scenario. Chen et al. employed CNN model to automatically learn feature for median filtering forensics and achieved great improvements for JPEG compressed image of low resolution.[10] Even so, its performance still needs to be improved when dealing with low resolution image undergone JPEG compression

The goal of this paper is to find a feature set with proper dimensionality to improve median filtering detector's performance in challenging problems, such as for strong JPEG compressed images or low-resolution images. To do this, median filtering residual is employed to expose the fingerprint left by median filtering. Two compensated models are employed to construct the proposed feature set. The first model is transition probability of Markov process, which is initially used for stegoanalysis.[11] It is useful to describe dependence among adjacent residuals at small value elements. In the literature of stegoanalysis, the residual component is always truncated into a low range, such as [-3, 3], to reduce the dimensionality of feature. These truncation operations lose a little information in stegoanalysis, as steganographic methods cause minor changes at cover pixels. But when employ transition probability model for median filtering forensics, truncation may influence detector's performance because the truncated part has some median filtering statistical fingerprints. The AR model, whose coefficients are sensitive to large residual elements, is employed to compensate the lack of transition probability caused by truncation. Experimental results on a large composite database demonstrate that the proposed detector not only performs well in ideal condition, but also displays good generalization ability that is useful in practical applications.

This paper is an extension of our previous work.[1] Several novelties are added in this paper: (1) verifying the superiority of median filtering residual to the first-order difference by elaborate experiments; (2) exploring compensated effect between AR model and transition probability and incorporating them to construct the proposed feature set; (3) estimation of generalization ability on heterogeneous image sources.

The rest of this paper is organized as follows. In Section 2, the statistical properties of median filtering residual are analyzed, and then the construction of proposed feature set is introduced. Experimental results are reported in Section 3. Finally, the conclusion is drawn in the end.

In the following sections, some symbols are used as follows. The capital-case symbol X represents an image with size $M \times N$. The symbol MF3 and MF5 represent the median filtering image using 3×3 and 5×5 filtering window respectively. "JPEG 70" denotes the image processed by JPEG compression with quality factor 70 and "MF3+JPEG 70" denotes the composite operation of median filtering followed by JPEG 70. The symbol "JPEG 70 VS MF3+JPEG 70" denotes a training-testing pair composed by JPEG 70 images (negative class) and MF3+JPEG 70 images (positive class). For any real number u, the operation $[u]$ stands for the least integer which is larger than u.

2. PROPOSED DETECTION METHOD

For the median filtering detection task, how to analyze the median filtering fingerprints and how to describe the fingerprints by a proper feature set are two key points. To address these two important issues, statistical properties of median filtered residual are first used to analyze statistical fingerprints of median filtering, and then a composite feature set based on median filtering residual are constructed.

2.1 Median filtered Residual

The median filter replaces central pixel's intensity with the median value of pixels in a $w \times w$ window. 2-D median filter is performed as (1) for a pixel $X(i, j)$.

$$Y(i,j) = med_w(X(i,j)), 1 \le i \le M, 1 \le j \le N \quad (1)$$

where w is the filtering window size.

The median filtering residual (MFR) is a proper residual to eliminate influence from image content, which is effective in median filtering detection.[1] The MFR of pixel $X(i,j)$ is defined as (2):

$$R(i,j) = med_w(X(i,j)) - X(i,j) = Y(i,j) - X(i,j) \quad (2)$$

where $Y(i,j)$ is the median value at point (i,j). We set w = 3 to get MFR for each pixel in practice. After executing the formula (2) on the whole image X, we can get a MFR matrix $R \in \mathbf{R}^{M \times N}$.

The smoothing effect of median filtering make MFR illustrates some distinctive properties on median filtering image.

Specially, MFR matrix of filtered image (R^1) has much more zero elements than MFR matrix R^0 of un-altered image (R^1) as shown in Figure 1(a). Suppose Z is the second MF3 version of original image X, i.e. $Z(i,j) = med_3(Y(i,j))$. The first median filter makes smooth region of X show nearly constant value in Y. Meanwhile, texture region in Y tends to become median value in its 3×3 support, which is called block median.[4] So again performing median filtering on Y makes $Z(i,j)$ be equal with $Y(i,j)$ with high probability, thus produce many zero elements in R^1. A close inspection of Figure 1(a) also tells us that there are significant differences at large absolute MFR elements, such as MFR$\geq$5. As a larger filtering window resulting in more smoothly image, MFR of MF5 shows more clear distinction than that of MF3 in Figure 1. The same conclusion can be drawn for JPEG 50 images as shown in Figure 1(b). However, the gap between filtered and un-altered image has become smaller, which indicates that the post JPEG compression makes the median filtering forensic problem more challenging.

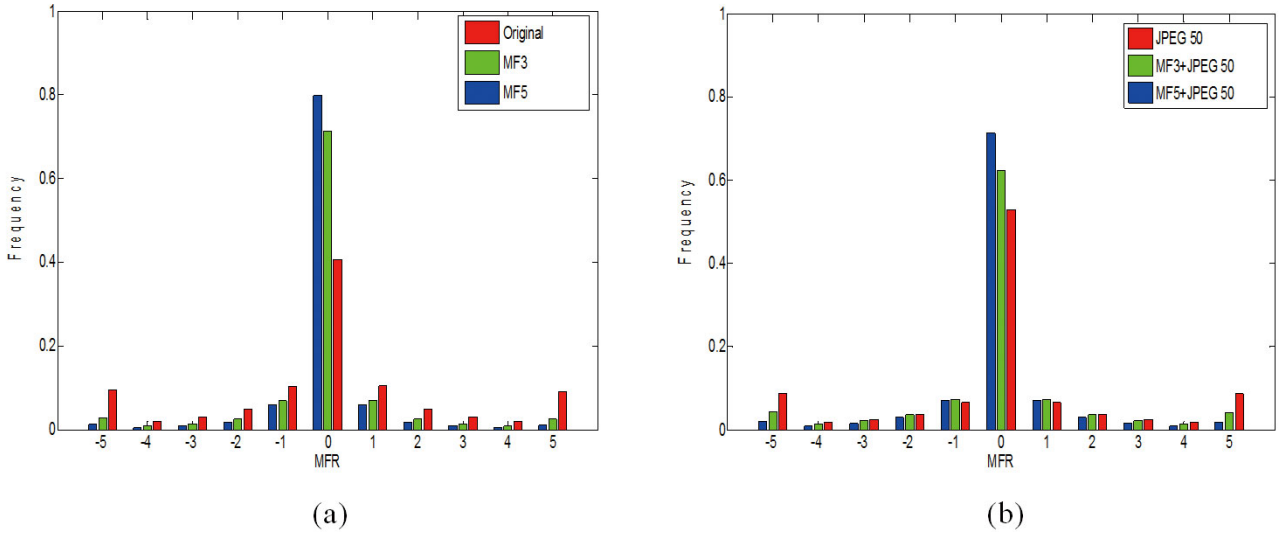

(a) (b)

Figure 1. The average histogram of MFR estimated from 6,690 images in a composite database for (a) un-compressed and (b) JPEG 50 compressed images. The x, y axis is the value of MFR and its frequency respectively. "Original" means un-altered image.

Median filtering is a locally window-based operator, which makes different relationships among neighboring pixels. MFR can be employed to reveal such different relationships. It can be supposed that the dependence among five consecutive MFRs of filtered image is stronger than that of original image. Two median filtering operations on $X(i,j)$ make $Z(i,j)$ originate from a 5×5 support of $X(i,j)$, thus five consecutive pixels of Z depend upon each other. Refer to un-altered image, only three consecutive residuals relate each other. We explicitly explain these different dependences by shared window.[1] This significant difference will be employed to construct new feature set in Section 3.

Compared to the commonly used first-order difference,[2,3,5] MFR eliminates interference from image content more thoroughly, especially for heavy JPEG compressed image. Due to the property that median filter keeps edge information, the extracted MFR contains a little edge information or block artifact caused by JPEG compression. It can be seen from Figure 2(c) that MFR contains fewer block artifacts than difference image (lines at sky region in Figure 2(b)). In the next section, we will construct feature set by transition probability of nth-order Markov chain for both MFR and first-order difference to compare their performance in the median filtering forensics.

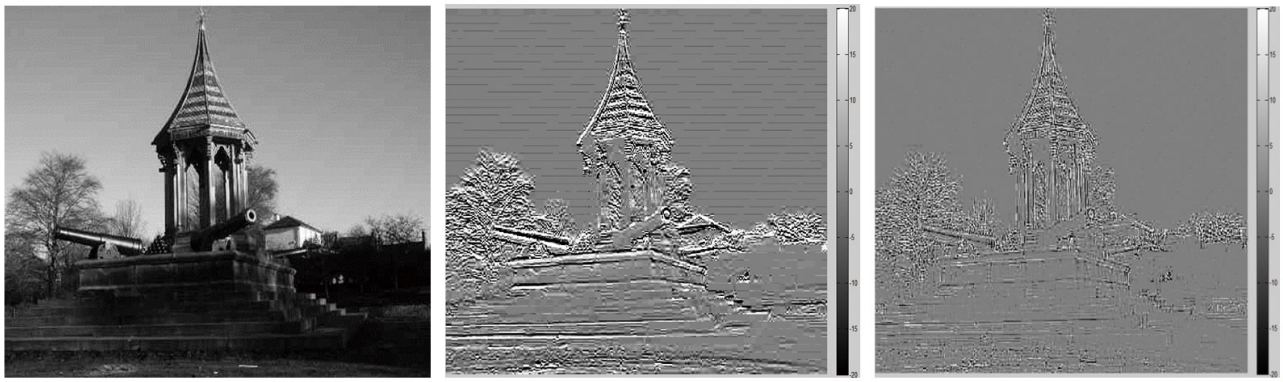

(a) (b) (c)

Figure 2. Example showing (a) JPEG 30 compressed image and (b) its vertical first-order difference image and (c) MFR image. For clear show, we specify display range of difference and MFR to [-20 20]. It is observed that there are fewer block artifacts in MFR image (lines at the sky) compared to difference image.

2.2 Feature extraction

In this section, we construct a new feature set on MFR (F_{MFR}). The first part of new feature set is constructed by transition probability of Markov chain. We call this feature set as F_M in the following. The calculation of F_M starts by computing MFR matrix (2). To avoid high dimensionality, MFRs are truncated into $[-T, T]$. After that, the procedure of calculating transition probability matrix of nth-order Markov chain is first calculating co-occurrence $C^{(h,v)}$ as (3) and then getting transition probability matrix $S^{(h,v)}$ as (4). If denominator in (4) is 0, we take that feature element as 0. The superscript (h, v) represents the direction of calculating transition probability. Four directions are considered: horizontal left to right and inverse, vertical top to bottom and inverse. That is, $(h, v) \in (0, 1), (0, -1), (1, 0), (-1, 0)$. F_M is obtained by averaging four direction's matrix $S^{(h,v)}$. The dimension of F_M is $(2T + 1)^{n+1}$.

$$R(i,j) = med_w(X(i,j)) - X(i,j) = Y(i,j) - X(i,j) \quad (3)$$

$$S^{(h,v)}(\alpha_1,...\alpha_{n+1}) = C^{(h,v)}(\alpha_1,...\alpha_{n+1}) / C^{(h,v)}(\alpha_2,...\alpha_{n+1}) \quad (4)$$

where $\alpha \in -T, \cdots, T, 1 \le i \le n$.

Though residual elements are truncated into $[-T, T]$, the dimensionality of F_M grows exponential when increasing chain order, so we further reduce the dimensionality of F_M based on symmetric characteristics of MFR. As shown in Figure 1, the histogram $H = \{h_{-255}, \cdots, h_0, \cdots, h_{255}\}$ of MFR is nearly symmetric about 0. Furthermore, the process of constructing F_M indicates F_M is rotation invariant, because $C^{(0,1)}(\alpha_1, \cdots, \alpha_n) = C^{(0,1)}(\alpha_n, \cdots, \alpha_1)$ and $C^{(1,0)}(\alpha_1, \cdots, \alpha_n) = C^{(-1,0)}(\alpha_n, \cdots, \alpha_1)$. Based on the above-mentioned symmetry and rotation invariance, dimensionality reduction version F_M^1 is executed as (5).

$$F_M^1(\alpha_1,...,\alpha_{n+1}) = (F_M(\alpha_1,...,\alpha_{n+1}) + F_M(-\alpha_1,...,-\alpha_{n+1}) + F_M(\alpha_{n+1},...,\alpha_1) + F_M(-\alpha_{n+1},...,-\alpha_1)) / 4 \quad (5)$$

After dimensionality reduction, the dimensionality of F_M^1 (denoted by $|F_M^1|$) is as follows:

$$|F_M^1| = \begin{cases} ((2T+1)^{\frac{n}{2}} + (2T+1)^{\frac{n+2}{2}} + (2T+1)^{n+1} + 1)/4, \text{if } n \text{ is even} \\ (2(2T+1)^{\frac{n+1}{2}} + (2T+1)^{n+1} + 1)/4, \text{if } n \text{ is odd} \end{cases} \quad (6)$$

It can be inferred from (6) that the dimensionality of F_M^1 is decided by the order of Markov chain n and truncated threshold value T. A trade-off between detection accuracy and the dimensionality is balanced by adjusting these two parameters. According to the discussion in the Section II.A, five consecutive MFR residuals of median filtering image embody a certain degree of dependence. So, we employ 4th-order (n = 4) Markov chain to reveal such different dependence among

neighboring residuals. Experimental results in Table 1 will empirically verify that 4th-order (n = 5) Markov chain is a proper choice. To reduce dimensionality, MFR is truncated into [-1, 1]. After transferring transition probability matrix to feature vector, the dimension of first part of FMFR is 70-D.

Table 1. Comparison results (Dimension, Acc (%)) between MFR and first-order difference of MF3 detectors on the composite database. The feature set F_M^1, F_D^1 is the dimensionality reduction version of F_D, F_M respectively. The best result for each experiment (by row) is displayed with bold texts.

	JPEG 70				**JPEG 50**			
	$\boldsymbol{F_D}$	$\boldsymbol{F_M}$	F_D^1	F_M^1	$\boldsymbol{F_D}$	$\boldsymbol{F_M}$	F_D^1	F_M^1
n=2,T=2	250,94.1	125, **95.6**	78,94.0	39, 95.4	250,88.4	125, 93.0	78, 88.6	39, **93.0**
n=2,T=3	686, 96.1	343, **96.7**	200, 96.1	100, 96.6	686, 91.4	343, 93.9	200, 92.1	100, **94.2**
n=3,T=1	162, 96.5	81, **97.4**	50, 96.3	25, 97.3	162, 93.6	81, **95.3**	50,93.7	25, 95.1
n=3,T=2	1250,97.8	625, 97.9	338, 97.9	169, **98.2**	1250, 94.5	625, **95.9**	338, 94.8	169, 95.9
n=4,T=1	486, 97.8	243, 98.4	140, 97.8	70, **98.4**	486- 94.8	243, 95.6	140, 95.0	70, **95.9**
n=4,T=2	-----	-----	1638, 98.1	819, **98.3**	-----	-----	1638, 95.1	819, **95.7**
n=5,T=1	-----	-----	392, 98.0	196, **98.0**	-----	-----	392, 95.6	196, **96.5**

The transition probability matrix explicitly describes neighboring dependence at residual elements with small value -1, 0, 1. However, it ignores the dependence among elements whose absolute value is larger than 1 due to truncation of MFR, whereas the distribution of residual elements with large value is also distinctive as shown in Figure 1. To compensate lost information caused by truncation, we employ coefficients of 10-order AR model as the second part of new feature set. After changing MFR matrix R into column vector R^v, the AR model describes dependence among neighboring residual elements as (7), where p is the order, l is the length of R and $\epsilon(i)$ is the stochastic error. It can be inferred from the formula (7) that AR coefficient $\phi(j)$, $1 \leq j \leq p$ is sensitive to large MFR element. We further explain it by Yule-Walker equations, which can be used to estimate AR coefficients. In the formula (8), $\gamma(m)$, $1 \leq m \leq p$ is the auto-correlation and its unbiased estimator is shown in the formula (9). It can be inferred from (9) that large residual elements cause significantly changes on $\gamma(m)$. These changes will transfer to AR coefficients through linear equations (8), so $\phi(j)$ is sensitive to large MFR value. When calculating AR coefficients, no truncation is executed on MFR, thus AR coefficients keep information about MFR elements with large absolute value. On the other hand, we can also suppose that AR coefficient is not sensitive to small value elements from (9) and (10). The flaw of AR model at small value element can be compensated by transition probability.

$$R^v(i) = \sum_{j=1}^{p} \phi(j) R^v(i-j) + \varepsilon(i), \; p+1 \leq i \leq l \tag{7}$$

$$r(m) = \sum_{j=1}^{p} \phi(j) y(m-j), 1 \leq m \leq p \tag{8}$$

$$r(m) = \frac{1}{l-m} \sum_{t=1}^{l-m} R^v(t) R^v(t+m), 1 \leq m \leq p \tag{9}$$

In summary, FMFR is composed by F_M^1 (n = 4, T = 1) and 10-order AR coefficients and the final dimensionality is 80. To visually demonstrate detection ability of F_{MFR}, scatter plots of three elements are shown in Figure 3. These three elements get the top three Fisher Criterion Score (FCS), which is a measurement of single feature element's detection ability as defined in (10),

$$FCS(k) = (u_k^1 - u_k^0)^2 / ((\sigma_k^1)^2 + (\sigma_k^0)^2) \tag{10}$$

where $u_k^1(u_k^0)$ is the mean of k^{th} element of median filtering (original) class and $\sigma_k^1(\sigma_k^0)$ is respective standard variance. When calculate FCS on BOWS2[12] database, the top three elements are selected: F_M^1(1,-1,-1,1,-1), F_M^1(0,1,1,-1,-1) and the 3^{rd} coefficient $\phi(3)$ of AR model. The left plot of Figure 3 demonstrates that these three elements behave clear distinction for un-compressed images. For JPEG compression scenario shown in the right plot of Figure 3, though there are some overlapping regions between JPEG 70 compressed and MF3+JPEG 70 compressed images, it is expected that all elements of FMFR will achieve excellent performance in median filtering forensics.

ISSN 2577-7742 E-ISSN 2577-7769

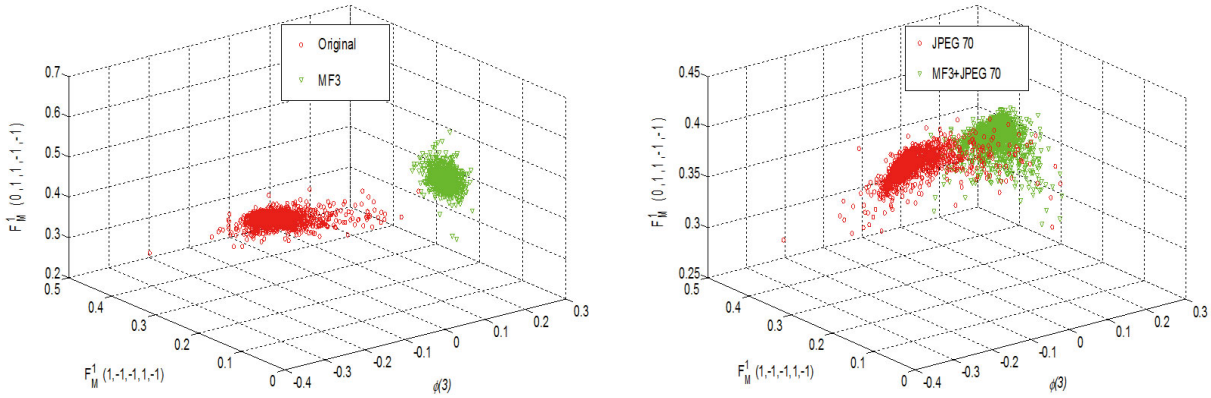

Figure 3. The scatter plots of the top three FCS score elements estimated from 1,338 un-compressed (left) and JPEG 70 compressed (right) images of BOWS2 database

3. EXPERIMENTAL RESULTS

A composite image database containing 6,690 images is employed to evaluate the performance of the proposed feature set. These images are from five image databases: the BOSS RAW database (BR),[13] the BOWS2 image database (BOWS2),[12] the Dresden Image Database (DID),[14] the NRCS Photo Gallery (NRCS)[15] and the UCID database.[16] Each database contributes 1,338 images. The size of image from UCID is 512 $\times$ 384, while images from other four databases are 512 $\times$ 512 by cropping central part of source image. All 6,690 images are converted to 8-bit gray images before any further processing.

SVM with RBF kernel is chosen as binary classifier.[17] A grid-search for best parameter C and γ is conducted by five-fold cross validations. The negative class is the original composite database and the positive class is the median filtering version of composite database. Both classes followed by different JPEG compressions are used to evaluate robustness of proposed method against JPEG compression. We call the composition of negative class and positive class by training-testing pair. The cardinality of training set is a half of two classes and the other half is the testing set. Hereafter, the same experimental settings is adopted unless specially mentioned. The median filtering detector is constructed by implementing SVM on each feature set. Detection accuracy (Acc) and receiver operating characteristic (ROC) curves on testing set are used to evaluate detector performance.

$$\text{Acc= \#correctly predicted samples/ \#total testing samples} \tag{11}$$

3.1 Empirical Comparisons of MFR and First-order Difference

We first evaluate performance of feature set based on MFR and first-order difference using transition probability. These two feature sets are denoted by F_M and F_D respectively. As indicated by Kirchner,[2] Besides of horizontal and vertical direction, diagonal and mirror diagonal directions are also considered when calculating F_D. The first half of F_D is formed by averaging the horizontal and vertical transition probability matrices and the rest half is the average value of diagonal and mirror diagonal transition probability matrices. Therefore, the dimension of F_D is $2(2T+1)^{n+1}$, which is two times of that of F_M. Feature sets under different chain orders n and truncated threshold values T are considered for thorough results. As the dimensionality of feature set with $n = 4$, $T = 2$ and $n = 5$, $T = 1$ is very large, we only show results of their dimensionality reduction version. For fair comparison, the experiments between F_M and F_D are performed with the same n and T. Since F_M and F_D achieved nearly perfect performance for un-compressed images,[1–5] we focus on images undergone JPEG 70 and JPEG 50 compression.

Experimental results in Table 1 show that both F_M and F_D achieve high detection accuracy on JPEG compressed images. The overall performance of F_M is better than that of F_D, even if the dimensionality of F_M is half of F_D under same conditions. The ROC of feature set using 3rd-order Markov process shown in Figure 4 also demonstrates the superiority of MFR. It can be seen hat curves of F_M (dashed line with triangle marker) are always above those of F_D (solid line). The same results can be obtained for other parameters.

We also evaluate the performance of dimensionality reduction version F_M^1 and F_D^1. Experimental results in Table 1 again demonstrate that the performance of F_M^1 is superior to that of F_D^1 under the same parameter. Comparing original feature set with its dimensionality reduction version, the performance of $F_M^1(F_D^1)$ is comparable with that of $F_M(F_D)$, however the dimensionality of $F_M^1(F_D^1)$ is about 1/3 of its

origin. These results empirically verify the efficacy of dimensionality reduction method. Experimental results in each column of Table 1 tell us that increasing the order of Markov chain benefits more in detection accuracy than increasing truncated value. For example, both F_M and F_D using 3rd-order Markov chain with T = 1 is better than using 2^{nd}-order chain with T = 3, although the dimensionality of the former is about 1/4 of the latter.

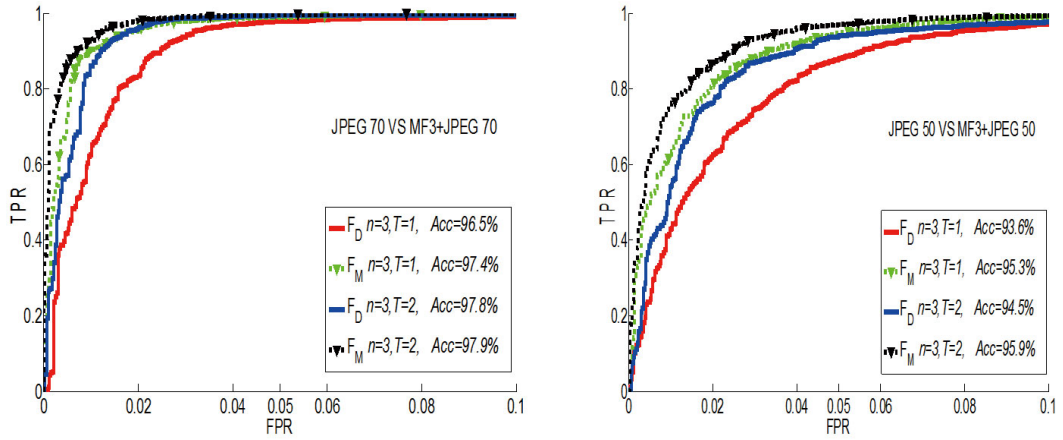

(a) (b)

Figure 4. ROC curves of MF3 detectors using 3rd-order Markov chain with T = 1, 2 for (a) JPEG 70 and (b) JPEG 50 images on the composite database

3.2 Comparison Proposed Method with Prior Arts

To fairly compare F_{MFR} with the state-of-the-art, including the AR method (10-D),[1] GLF method (56-D)[5] and the 2DAR method (81-D),[9] the same experimental setups are employed. The feature set obtained from transition probability F_M^1 ($n = 4, T = 1$, 70-D) is added to verify complementary effect between transition probability and AR model.

The first kind of experiment is designed for the baseline test that training images and testing images are from the same source. The un-compressed, JPEG 90 and JPEG 70 compressed images as well as low resolution images are considered for this kind experiment. Detailed results are shown in Table 2. It can be seen that all methods achieve perfect performance for the un-compressed image of full size (512 × 512, 512 × 384). For the JPEG 90 and JPEG 70 compressed images of full size, FMFR achieves the best detection performance and outperforms AR and GLF a lot.

Table 2. Detection accuracy (%) of MF3 detector for all methods. "Without JPEG" means un-compressed images. The best result for each is displayed by bold texts.

	Without JPEG				**JPEG 90**				**JPEG 70**			
	Full size	**128 × 128**	**64 × 64**	**32 × 32**	**Full size**	**128 × 128**	**64 × 64**	**32 × 32**	**Full size**	**128 × 128**	**64 × 64**	**32 × 32**
AR	99.8	96.0	93.6	88.9	98.2	94.2	90.1	82.0	95.8	88.1	81.6	74.2
GLF	100	99.8	99.7	**99.4**	98	93.9	90.0	86.4	94.3	86.1	82.2	**77.2**
F_M^1	100	99.8	99.6	99.0	99.6	97.9	93.5	86.4	98.4	91.3	84.4	76.5
2DAR	99.9	99.1	98.4	96.8	99.5	97.6	93.9	85.7	97.5	91.9	**85.5**	74.6
F_{MFR}	**100**	**99.9**	**99.8**	99.0	**99.6**	**98.2**	**94.2**	**87.9**	**98.8**	**92.2**	84.6	**77.2**

We then design experiments for low resolution images. To prepare training-testing pairs, we create small composite databases by cropping 128 × 128, 64 × 64 and 32 × 32 blocks from central part of each image in the composite database respectively. For un-compressed images, FMFR and GLF method achieve nearly perfect performance, but AR method deteriorates with decreasing image size. For JPEG compressed images, experimental results show that the performance of all four methods decrease drastically when the resolution drops from 128 × 128 to 32 × 32. This is

ISSN 2577-7742 E-ISSN 2577-7769

because small resolution image results in weak statistical fingerprints. Improving detection ability on small size image with JPEG compression is our future work, which is useful in tampering detection. It also can be seen that FMFR consistently outperforms (70-D) and 10-order AR detector, which empirically verify that transition probability and AR model compensate each other.

In practical applications, it is probably that test images and trained images are not from the same image source, so we test generalization ability of all methods in the second experiment. In this situation, testing images are heterogeneous with training images. To approximate practical applications, different resolutions and filtering window sizes are considered. Explicitly speaking, the original image set is composed by three kinds of resolution image (256×256, 128×128 and its original size in the composite database). Besides resolution factor, two kinds of filtering window (3×3 and 5×5) are employed for median filtering image set. As large filtering window (7×7, 9×9 etc.) results in visually blurred image, we don't consider them. In this experiment, training samples are from four image databases and the remaining fifth image database is the testing set. The training set consists of 5,352 un-filtered and 5,352 median filtered images, while the testing set contains 1,338 un-filtered and 1,338 median filtered images. For un-compressed images, experimental results in Table 3 demonstrate that FMFR and GLF method achieve nearly perfect performance. The performance of AR method is also good for four testing databases except for BR database.

For JPEG compressed images, the mismatch between training set and testing set decreases performance of each detector, but FMFR also achieves the best performance. All detectors deteriorate sharply when testing images from BR database. Some images from BR are very smooth and saturated, so they are more challenging. The experimental result in Table 3 demonstrates that our proposed method behaves excellent generalization ability.

Table 3. Detection accuracy (%) of detectors on generalization ability test for image of full size. Database in column is the source of testing images and the rest four databases compose the training set. "Without JPEG" represents un-compressed images.

	Without JPEG					**JPEG 70**				
	BR	**BOWS2**	**DID**	**NRCS**	**UCID**	**BR**	**BOWS2**	**DID**	**NRCS**	**UCID**
AR	87.2	98.7	92.7	95.0	94.1	78.1	94.1	88.9	90.9	89.6
GLF	99.4	99.6	99.2	99.9	**100**	78.6	93.5	87.4	89.4	91.3
2DAR	99.4	99.7	99.7	99.8	99.6	86.9	95.8	92.0	95.0	94.6
F_{MFR}	**99.5**	**99.9**	**99.7**	**100**	99.3	**88.7**	**97.2**	**93.0**	**95.7**	**95.6**

4. CONCLUSION

In this paper, an improvement approach which is based on Markov chain and AR model is proposed to detect median filtering in challenging problems, such as strong JPEG compressed images and low-resolution images. To do this, we thoroughly discuss the parameters of Markov model, including chain order n and truncated threshold T, and find that the detection accuracy increases when increasing chain order from 2 to 4. The larger order chain ($n > 4$) benefits little from detection accuracy but with higher dimensionality resulted in huge computational burden in SVM classification. For a feature set with proper dimension, 4^{th}-order Markov chain with $T = 1$ is used in practice. A dimensionality reduction method is developed to further lower the dimensionality. One of the contributions of our work is exploring compensated effect between transition probability and AR model and incorporating them to construct the proposed feature set. A large number of experiments demonstrate that our proposed detector outperforms prior arts a lot. Even for the challenging generalization ability test, the proposed detector also achieves high detection accuracy. In the future, we would like to design a more applicable detector by using different model.

ACKNOWLEDGEMENTS

This work was partially supported by NSFC (Grant No. 61702429), the Scientific Research of Sichuan Provincial Education Department (Grant No. 17ZB0450), Doctoral Research Fund of Southwest University of Science and Technology (Grant No. 16zx7104) and the Fund of Fundamental Sichuan Civil-military Integration Institute.

REFERENCES

[1] Kang X, Stamm MC, Peng A, Liu KJR. Robust median filtering forensics using an autoregressive model. IEEE Trans. Inf. Forensics Security. 2013; 8(9): 1456-1468. https://doi.org/10.1109/TIFS.2013.2273394

[2] Kirchner M, Fridrich J. On detection of median filtering in digital images. In Proc. SPIE, Electronic Imaging, Media Forensics and Security II in Human Behavior. 2010; 7541: 1-12. https://doi.org/10.1117/12.839100

[3] Cao G, Zhao Y, Ni R, Yu L, Tian H. Forensic detection of median filtering in digital images. In Proc. 2010 IEEE Int. Conf. Multimedia and EXPO 2010. 2010: 89-94. https://doi.org/10.1109/ICME.2010.5583869

[4] Yuan H. Blind forensics of median filtering in digital images. IEEE Trans. Inf. Forensics Security. 2011; 6(4): 1335-1345. https://doi.org/10.1109/TIFS.2011.2161761

[5] Chen C, Ni J, Huang R, Huang J. Blind median filtering detection using statistics in difference domain. In Proc. of information Hiding 2012, Berkeley, USA. 2012: 14-22. https://doi.org/10.1007/978-3-642-36373-3_1

[6] Popescu AC, Farid H. Exposing digital forgeries by detecting traces of resampling. IEEE Transactions on Signal Processing. 2005; 53(2): 758-767. https://doi.org/10.1109/TSP.2004.839932

[7] Luo W, Huang J, Qiu G. JPEG error analysis and its applications to digital image forensics. IEEE Trans. Inf. Forensics Security. 2010; 5(3): 480-491. https://doi.org/10.1109/TIFS.2010.2051426

[8] Bovik AC. Streaking in median filtering images. IEEE Transactions on Acoustics. Speech and Signal Processing. 1987; 35(4): 493-503. https://doi.org/10.1109/TASSP.1987.1165153

[9] Yang J, Ren H, Zhu GP, Huang JW, Shi YQ. Detecting median filtering via two dimensional AR models: Multimedia Tools and Applications. 2017; (4): 1-23. https://doi.org/10.1007/s11042-017-4691-0

[10] Chen J, Kang X, Liu Y, Wang ZJ. Median filtering forensics based on convolutional neural networks: IEEE Signal Process Letters. 2015; 22(11): 1849-1853. https://doi.org/10.1109/LSP.2015.2438008

[11] Pevný T, Bas P, Fridrich J. Steganalysis by subtractive pixel adjacency matrix: IEEE Trans. Inf. Forensics Security. 2010; 5(2): 215-224. https://doi.org/10.1109/TIFS.2010.2045842

[12] Bas P, Furon T. Break Our Watermarking System. 2nd ed. 2005. Available from: http://bows2.ec-lille.fr/

[13] Bas P. Available from: http://exile.felk.cvut.cz/boss/BOSSFinal/index.php?mode=VIEW&tmpl=materials

[14] Schaefer G, Stich M. UCID-An uncompressed color image database. In Proceedings of SPIE, Storage and Retrieval Methods and Applications for Multimedia. 2004: 472-480. https://doi.org/10.1117/12.525375

[15] United States Department of Agriculture. Natural resources conservation service photo gallery. Available from: http://photogallery.nrcs.usda.gov

[16] Gole T, Bohme R. Dresden Image Database for benchmarking digital image forensics. In Proceedings of the 2010 ACM Symposium on Applied Computing. 2010: 22-26. https://doi.org/10.1145/1774088.1774427

[17] Chang CC, Lin CJ. LIBSVM: a library for support vector machines: ACM Transactions on Intelligent Systems and Technology. 2011: 27-38. https://doi.org/10.1145/1961189.1961199